Acta Crystallographica Section D
Biological Crystallography
ISSN 0907-4449

Structural analysis of human dihydrofolate reductase as a binary complex with the potent and selective inhibitor 2,4-diamino-6-{2′-*O*-(3-carboxypropyl)oxydibenz[*b*,*f*]-azepin-5-yl}methylpteridine reveals an unusual binding mode

Vivian Cody,[a,b]* Jim Pace[a] and Jessica Nowak[a]

[a]Structural Biology Department, Hauptman–Woodward Medical Research Institute, 700 Ellicott Street, Buffalo, NY 14203, USA, and [b]University of Buffalo, Buffalo, NY 14260, USA

Correspondence e-mail: cody@hwi.buffalo.edu

Received 26 May 2011
Accepted 25 July 2011

PDB Reference: hDHFR complex, 3s7a.

In order to understand the structure–activity profile observed for a series of substituted dibenz[*b*,*f*]azepine antifolates, the crystal structure of the binary complex of human dihydrofolate reductase (hDHFR) with the potent and selective inhibitor 2,4-diamino-6-{2′-*O*-(3-carboxypropyl)oxydibenz[*b*,*f*]-azepin-5-yl}methylpteridine (PT684) was determined to 1.8 Å resolution. These data revealed that the carboxylate side chain of PT684 occupies two alternate positions, neither of which interacts with the conserved Arg70 in the active-site pocket, which in turn hydrogen bonds to water. These observations are in contrast to those reported for the ternary complex of mouse DHFR (mDHFR) with NADPH [Cody *et al.* (2008), *Acta Cryst.* D**64**, 977–984], in which the 3-carboxypropyl side chain of PT684 was hydrolyzed to its hydroxyl derivative, PT684a. The crystallization conditions differed for the human and mouse DHFR crystals (100 m*M* K_2HPO_4 pH 6.9, 30% ammonium sulfate for hDHFR; 15 m*M* Tris pH 8.3, 75 m*M* sodium cacodylate, PEG 4K for mDHFR). Additionally, the side chains of Phe31 and Gln35 in the hDHFR complex have a single conformation, whereas in the mDHFR complex they occupied two alternative conformations. These data show that the hDHFR complex has a decreased active-site volume compared with the mDHFR complex, as reflected in a relative shift of helix *C* (residues 59–64) of 1.2 Å, and a shift of 1.5 Å compared with the ternary complex of *Pneumocystis carinii* DHFR (pcDHFR) with the parent dibenz[*b*,*f*]azepine PT653. These data suggest that the greater inhibitory potency of PT684 against pcDHFR is consistent with the larger active-site volume of pcDHFR and the predicted interactions of the carboxylate side chain with Arg75.

1. Introduction

Recent structure–activity data have shown that dibenz[*b*,*f*]-azepines such as PT653 (Fig. 1) are moderately selective against *Pneumocystis carinii* dihydrofolate reductase (pcDHFR; Rosowsky *et al.*, 1999), the target for treatment of *Pneumocystis* pneumonia (Kovacs *et al.*, 2002). These studies led to the structure-based design of a series of 2,4-diamino-6-{(ω-carboxyalkyl)oxydibenz[*b*,*f*]azepin-5-yl}pteridines that were more potent and selective than trimethoprim (TMP) or piretrixim (PTX) (Fig. 1) as inhibitors of DHFR from opportunistic pathogens such as *P. carinii*, *Toxoplasma gondii* or *Mycobacterium avium* (Rosowsky *et al.*, 2004; Chan *et al.*,

2005). These studies revealed that the 2′-*O*-(3-carboxypropyl) analogue (PT684; Fig. 1) had the greatest inhibitory potency against pcDHFR, with an IC_{50} of 1.1 n*M* and a selectivity ratio of 1300 when compared with rat liver DHFR (IC_{50} = 1500 n*M*). These data further suggested that modification of the 2′-position of the dibenz[*b*,*f*]azepine ring contributed significantly to defining selectivity for the pathogenic DHFR enzymes. Previously reported computational models of the binding of PT684 in both human DHFR (hDHFR) and pcDHFR showed the influence of hydrogen-bond interactions between the carboxylate of PT684 and Lys37 and Arg75 in enhancing antifolate selectivity for pcDHFR. Similar interactions have been proposed for Arg70 of hDHFR, but with a weaker contribution from Gln35 (Rosowsky *et al.*, 2004).

Structural studies of the mouse DHFR (mDHFR) complex with PT684 and NADPH could not validate the computational binding data for PT684 as this inhibitor had hydrolyzed to the hydroxyl analogue PT648a (Fig. 1) under the crystallization conditions used (15 m*M* Tris pH 8.3, 75 m*M* sodium cacodylate, PEG 4000; Cody *et al.*, 2008). The crystal structure of PT684 in complex with hDHFR was obtained in order to understand these structure–activity correlations. These data are compared with previously reported structural data of PT684a in complex with mDHFR (Cody *et al.*, 2008) and the parent compound PT653 (Fig. 1; Cody *et al.*, 2002).

2. Methods

2.1. Expression of hDHFR

Recombinant hDHFR was expressed in a pET-SUMO-DHFR plasmid which contained a His tag for Ni-column

Table 1
Data-collection and refinement statistics for hDHFR–PT684.

Values in parentheses are for the highest resolution shell.

Data collection	
Space group	$P2_12_12_1$
Unit-cell parameters (Å)	a = 55.17, b = 54.79, c = 64.90
Beamline	SSRL 9-2
Resolution (Å)	1.83
Wavelength (Å)	0.975
R_{merge}	0.098 (0.25)
R_{sym}† (%)	0.10 (0.26)
Completeness (%)	96.7 (81.1)
Observed reflections	117176 (10039)
Unique reflections	17302 (2040)
$\langle I/\sigma(I)\rangle$	13.7 (4.8)
Multiplicity	6.8 (4.9)
Refinement and model quality	
Resolution range (Å)	42.0–1.83
Observed reflections (%)	96.4
No. of reflections	16381
R factor‡	21.8
R_{free}§	24.1
Total protein atoms	1680
Total water atoms	46
Average *B* factor (Å^2)	28.5
Error in Luzzati plot	0.236
R.m.s. deviation from ideal	
Bond lengths (Å)	0.022
Bond angles (°)	2.055
Ramachandran plot	
Residues in most favored regions (%)	97.3
Residues in additional allowed regions (%)	2.7
Residues in generously allowed regions (%)	0.0
Residues in disallowed regions (%)	0.0
PDB code	3s7a

† $R_{sym} = \sum_{hkl}\sum_i |I_i(hkl) - \langle I(hkl)\rangle|/\sum_{hkl}\sum_i I_i(hkl)$, where $\langle I(hkl)\rangle$ is the mean intensity of a set of equivalent reflections. ‡ *R* factor = $\sum_{hkl} ||F_{obs}| - |F_{calc}||/\sum_{hkl}|F_{obs}|$, where F_{obs} and F_{calc} are observed and calculated structure-factor amplitudes. § R_{free} was calculated as for the *R* factor for a random 5% subset of all reflections.

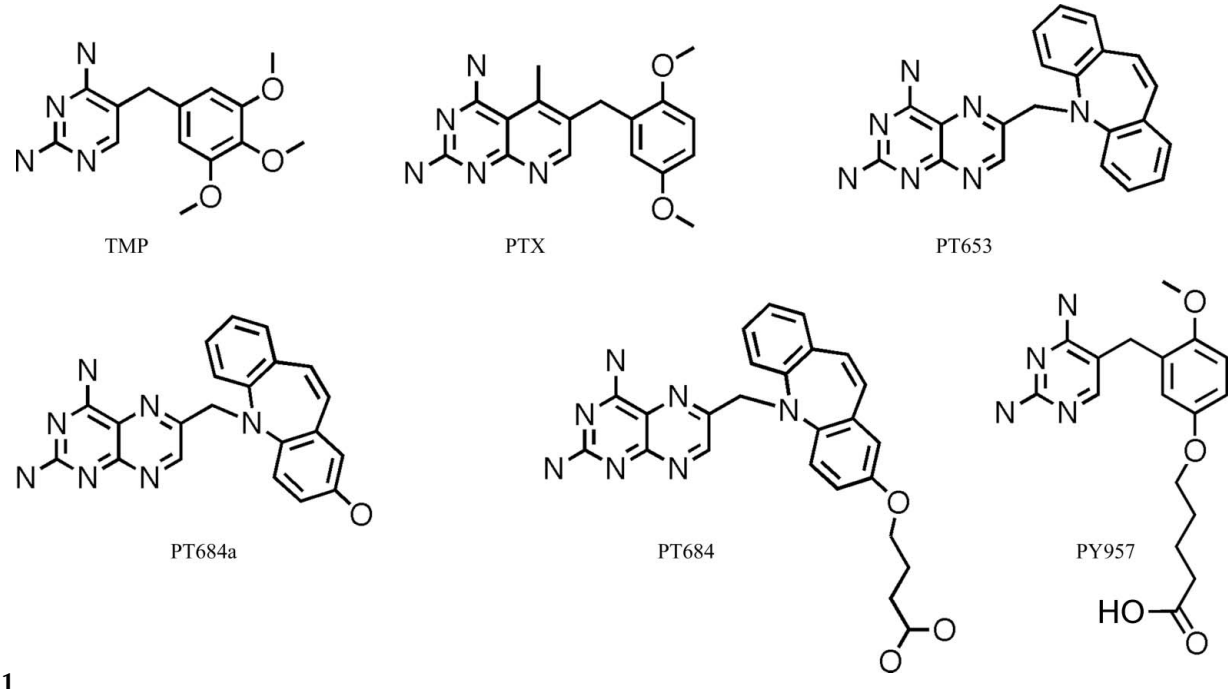

Figure 1
Schematic representations of the antifolates under study.

purification. The tag was removed by SUMO protease cleavage as described previously (Cody *et al.*, 2009). The hDHFR was further purified by size-exclusion chromatography (G75 gel-filtration column, GE Healthcare).

2.2. Crystallization

The protein was concentrated to 5.4 mg ml^{-1} and incubated with a 10:1 molar excess of NADPH and a 10:1 molar excess of the inhibitor 2,4-diamino-6-{2′-*O*-(3-carboxylpropyl)oxydibenz[*b*,*f*]-azepin-5-yl}methylpteridine (PT684) for 1 h over ice prior to crystallization using the hanging-drop vapor-diffusion method. Protein droplets contained 30% ammonium sulfate in 100 m*M* K_2HPO_4 pH 6.9 and the reservoir contained 62% ammonium sulfate and 3% ethanol. Crystals were grown at 287 K using 10 µl drops on glass cover slips sealed with silicon grease. Data for the hDHFR complex with PT684 were collected on a Rigaku AFC111 Saturn 944+ CCD detector and were processed using *CrystalClear* (Rigaku). A higher resolution data set for this complex was also collected at the Stanford Synchrotron Radiation Lightsource (SSRL) and was processed using *MOSFLM* from the *CCP*4 suite of programs (Winn *et al.*, 2011); the final coordinates for this structure are reported in Table 1.

2.3. Structure determination

The structure of the hDHFR–PT684 binary complex was solved by molecular-replacement methods with *MOLREP* from the *CCP*4 program suite (Winn *et al.*, 2011) using the coordinates of hDHFR (PDB entry 1u71; Cody *et al.*, 2005). To monitor the refinement, a random subset of all reflections was set aside for the calculation of $R_{\rm free}$ (5%). Inspection of the resulting difference electron-density map was performed using the program *Coot* (Emsley & Cowtan, 2004) running on a Mac G5 workstation. The parameter file for the inhibitor was prepared using the Dundee *PRODRG*2 server website (http://davapc1.bioch.dundee.ac.uk/programs/prodrg; Schüttelkopf & van Aalten, 2004). The final cycles of refinement were carried out using *REFMAC*5 from the *CCP*4 program suite (Winn *et al.*, 2011). The Ramachandran conformational parameters from the last cycle of refinement generated by *RAMPAGE* (Lovell *et al.*, 2002) showed that more than 98% of the residues in the hDHFR binary complex have the most favored conformation and none are in the disallowed regions. The coordinates for this structure have been deposited with the Protein Data Bank (PDB entry 3s7a). Figures were prepared using the modeling program *PyMOL* (DeLano, 2002).

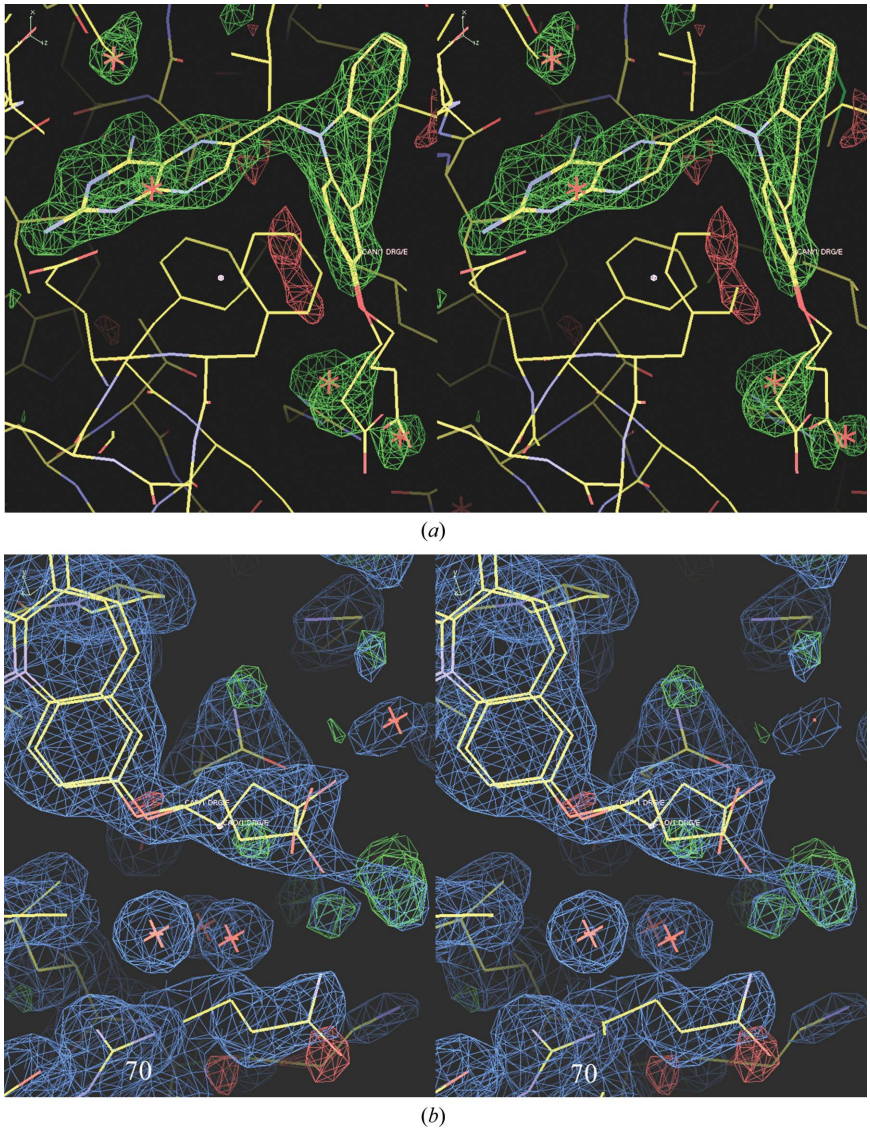

Figure 2
Stereoview of the difference electron density ($F_o - F_c$, 3σ) from the first molecular-replacement map for the hDHFR–PT684 complex. (*b*) Stereoview of difference electron density ($2F_o - F_c$, 1σ, blue) with the PT684 side chain refined at half occupancy. The position of Arg70 is marked for reference.

3. Results

Initial interpretation of the difference electron-density map suggested that the inhibitor was hydrolyzed to PT684a (Fig. 2*a*) as observed in the structure of the ternary complex of mDHFR with NADPH and PT684a (Cody *et al.*, 2008). However, further analysis revealed that the carboxylate side chain was present and refinement of the side chain at full occupancy showed that the thermal parameters for the carboxypropyl group were twice those of the rest of the molecule (35–45 Å^2 *versus* 15–20 Å^2). When the side chain was refined at half occupancy, positive density appeared in the electron-density map that could be fitted to two

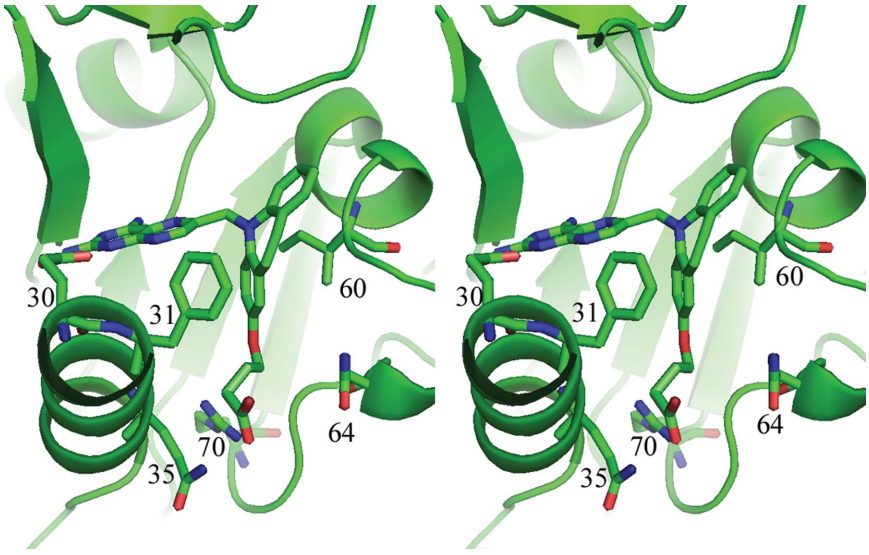

Figure 3
Stereoview of the hDHFR–PT684 binary complex, highlighting the active-site residues Glu30, Phe31, Gln35, Ile60, Asn64 and Arg70. Note that the carboxylate side chain of PT684 does not interact with Arg70.

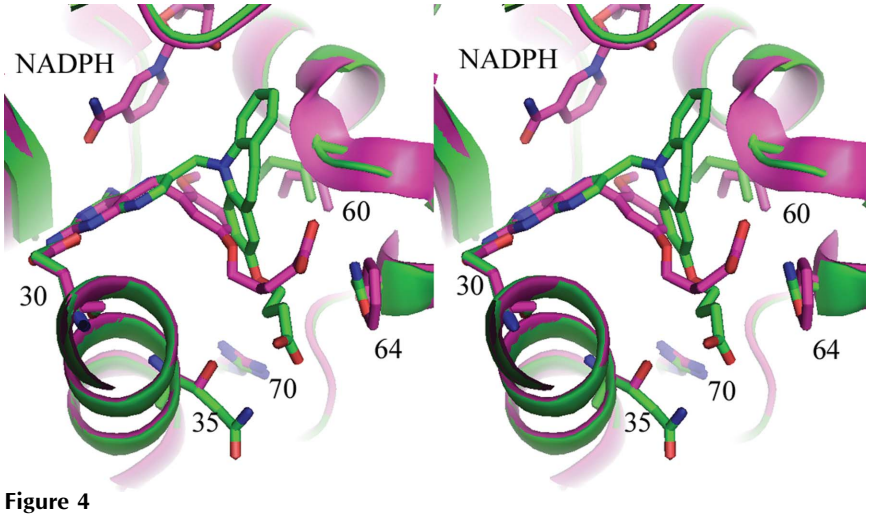

Figure 4
Stereoview of the hDHFR–PT684 binary complex (green) with that of the Q35S/N64F double mutant of hDHFR in a ternary complex with PY957 and NADPH (violet; Cody *et al.*, 2009). Note that the carboxylate side chains of these inhibitors do not interact with Arg70.

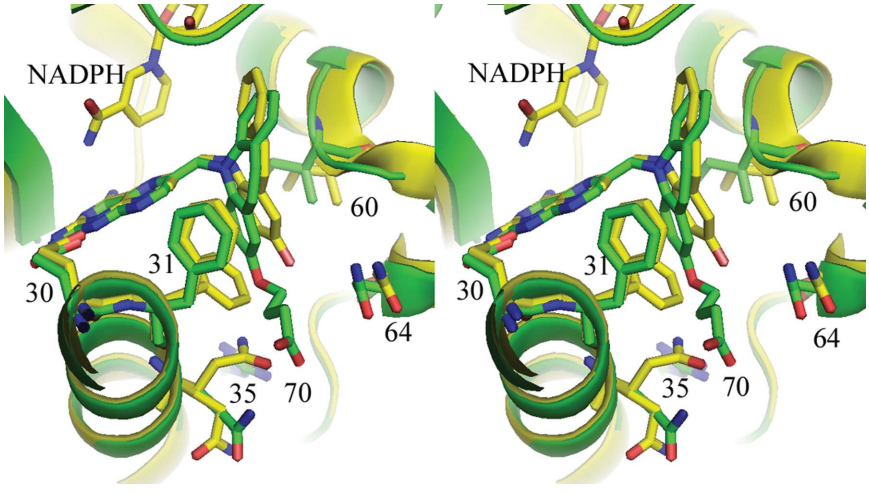

Figure 5
Stereoview of the binary complex of PT684 with hDHFR (green) and the ternary complex of mDHFR with NADPH and PT684a (yellow; Cody *et al.*, 2008). The active-site residues Glu30, Phe31, Gln35, Ile60 and Asn64 are shown. Note that Gln35 and Phe31 have two conformations in the mDHFR complex. Also note the displacement of the turn near Ile60 between hDHFR and mDHFR (1.2 Å).

alternate conformations of the side chain (Fig. 2*b*). These data also showed that the carboxylate side chain of PT684 does not interact with Arg70 as predicted by computational studies (Rosowsky *et al.*, 2004; Fig. 3). Instead, Arg70 interacts with water present in the active site and the carboxylate side chain of PT684 binds in an alternate position (Fig. 4), similar to that observed for the binding of PY957 (Fig. 1; Cody *et al.*, 2009). The side chain of Gln35 does make intermolecular contact with the carboxylate side chain of PT684. Additionally, only one conformer is observed for the side chains of Phe31 and Gln35 in the hDHFR binary complex, unlike the two conformers that are observed for these residues in the mDHFR–PT684a ternary complex (Cody *et al.*, 2008). In this structure, the side chain of Gln35 is pointing away from the active site and does not make contact with Arg70 as observed for one of the conformers in the mDHFR complex (Fig. 5).

Comparison of this complex with that of the parent dibenz[*b*,*f*]azepine PT653 (Fig. 1; Cody *et al.*, 2002; Figs. 5 and 6) revealed small variations in the buckling and tilt of the dibenz[*b*,*f*]azepine ring compared with the mDHFR or pcDHFR complexes (Cody *et al.*, 2002, 2008). These data also revealed that the backbone of helix *C* (encompassing residues 59–64; human numbering) is displaced by 1.5 Å (Ile60 C^{α} in hDHFR *versus* pcDHFR; Fig. 6) and by 1.2 Å for the mDHFR–PT684a complex (Fig. 5). These results are similar to the ligand-induced conformational changes observed in pcDHFR–folate complexes (Cody *et al.*, 1999). These data reveal that the shift in helix *C* of the PT684 binary complex causes the human enzyme to have the smallest active-site volume.

4. Discussion

This study describes the crystal structure of the binary complex of PT684 (Fig. 1) with hDHFR and reveals that the 3-carboxy-

propyl side chain of PT684 occupies two alternate positions, neither of which interacts with the conserved Arg in the active site. The mode of binding observed for nearly all folate ligands or inhibitors that incorporate a carboxylate moiety involves the formation of a salt bridge between the ligand carboxylate and the guanidinium ion of the conserved Arg in the active site (Cody & Schwalbe, 2006). One exception to this pattern was the alternate binding mode observed for PY957 (Fig. 4) in the crystal structure of the Q35S/N64F double mutant of hDHFR (Cody *et al.*, 2009). In this case, the N64F mutation and its juxtaposition to Phe31 in hDHFR resulted in the formation of a shallow hydrophobic pocket. The alternate binding mode for PY957 was stabilized by hydrophobic interactions between the methylene C atoms of the PY957 side chain and the side chains of Phe31 and Phe64 (Cody *et al.*, 2009).

The structural results for the binary complex of PT684 with hDHFR do not confirm the computational model for PT684 binding to hDHFR, which was based on the orientation of PT653 in the structure of pcDHFR (Cody *et al.*, 2002; Fig. 1) and which predicted carboxylate side-chain interactions with the conserved Arg70 (Rosowsky *et al.*, 2004). The crystal structure of the mDHFR complex with PT684 also could not confirm the computational binding models for PT684, as the results revealed that the 3-carboxypropyl side chain of PT684 was hydrolyzed to its hydroxyl derivative (PT684a; Fig. 1; Cody *et al.*, 2008).

To gain a better understanding of the potential interactions of the PT684 carboxylate side chain with Arg70 in hDHFR, a model based on the observed orientation of PT684 was generated by rotation of the carboxylate side chain towards Arg70. This model indicated that when the PT684 side chain is fully extended, the carboxylate group is positioned too close to the guanidinium of Arg70 (Arg70 NH$\cdots$PT684 COOH < 1.8 Å; Fig. 7). When the orientation of PT684 was mapped onto that of PT653 observed from the crystal structure of pcDHFR (Cody *et al.*, 2002), as was performed in the computational study, the contacts between the PT684 carboxylate and Arg70 are within normal hydrogen-bonding distances. Therefore, the crystal structure of PT684 in a binary complex with hDHFR shows that a change in the orientation of the dibenz[*b*,*f*]-azepin ring can play a significant role in the binding interactions of the 3-carboxypropyl moiety. These observations, together with those showing reduction in the active-site pocket as measured by the movement of helix *C* (residues 59–64), suggest that these data are consistent with the 1300-fold greater selectivity in binding of PT684 to pcDHFR (Rosowsky *et al.*, 2004).

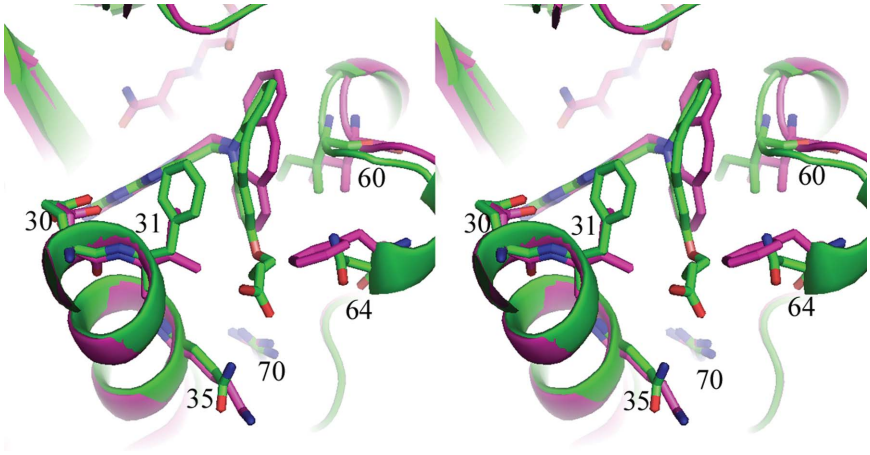

Figure 6
Stereoview of the hDHFR–PT684 binary complex (green) and the pcDHFR–PT653–NADPH ternary complex (violet; Cody *et al.*, 2002), highlighting the active-site residues Glu30, Phe31, Gln35, Ile60, Asn64 and Arg70. Note that the carboxylate of PT684 does not interact with Arg70. Also note the displacement of the turn near Ile60 between hDHFR and pcDHFR (1.5 Å).

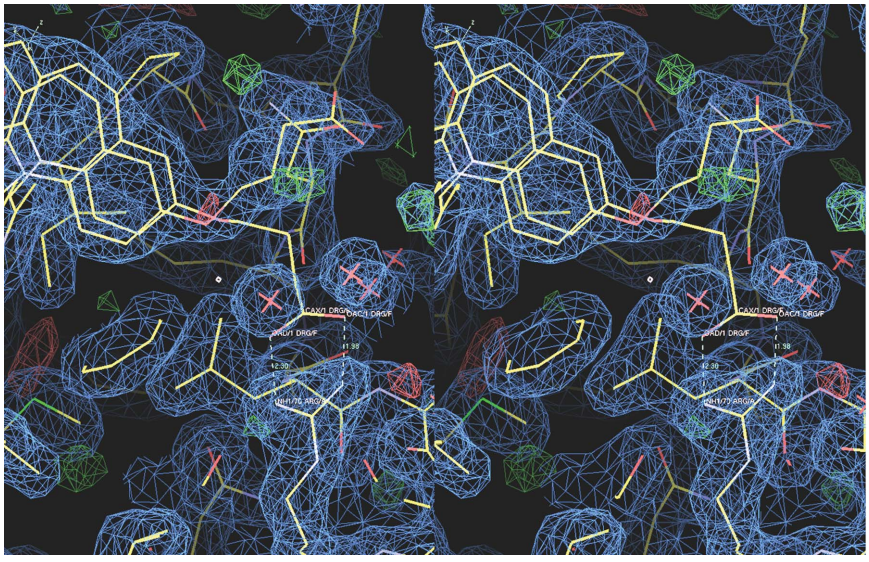

Figure 7
Stereoview of a hDHFR–PT684 electron-density difference map ($2F_o - F_c$, 1σ) with the side chain of one conformer modeled to interact with Arg70. Contact distances between the PT684 carboxylate and Arg70 are highlighted. The other conformer of PT684 follows the electron density that shows binding in an alternative position.

This work was supported in part by grants from the National Institutes of Health GM51670 (VC). The authors thank Dr Rosowsky for providing samples of PT684.

References

Chan, D. C., Fu, H., Forsch, R. A., Queener, S. F. & Rosowsky, A. (2005). *J. Med. Chem.* **48**, 4420–4431.

Cody, V., Galitsky, N., Luft, J. R., Pangborn, W., Rosowsky, A. & Queener, S. F. (2002). *Acta Cryst.* D**58**, 946–954.

Cody, V., Galitsky, N., Rak, D., Luft, J. R., Pangborn, W. & Queener, S. F. (1999). *Biochemistry*, **38**, 4303–4312.
Cody, V., Luft, J. R. & Pangborn, W. (2005). *Acta Cryst.* D**61**, 147–155.
Cody, V., Pace, J., Makin, J., Piraino, J., Queener, S. F. & Rosowsky, A. (2009). *Biochemistry*, **48**, 1702–1711.
Cody, V., Pace, J. & Rosowsky, A. (2008). *Acta Cryst.* D**64**, 977–984.
Cody, V. & Schwalbe, C. H. (2006). *Crystallogr. Rev.* **12**, 301–333.
DeLano, W. L. (2002). *PyMOL*. http://www.pymol.org.
Emsley, P. & Cowtan, K. (2004). *Acta Cryst.* D**60**, 2126–2132.
Kovacs, J. A., Gill, V. J., Meshnick, S. & Maur, H. (2002). *J. Am. Med. Assoc.* **286**, 2450–2460.
Lovell, S. C., Davis, I. W., Arendall, W. B. III, de Bakker, P. I. W., Word, J. M., Prisant, M. G., Richardson, J. S. & Richardson, D. C. (2002). *Proteins*, **50**, 437–450.
Rosowsky, A., Cody, V., Galitsky, N., Fu, H., Papoulis, A. T. & Queener, S. F. (1999). *J. Med. Chem.* **42**, 4853–4860.
Rosowsky, A., Fu, H., Chan, D. C. & Queener, S. F. (2004). *J. Med. Chem.* **47**, 2475–2485.
Schüttelkopf, A. W. & van Aalten, D. M. F. (2004). *Acta Cryst.* D**60**, 1355–1363.
Winn, M. D. *et al.* (2011). *Acta Cryst.* D**67**, 235–242.